Published in final edited form as:
JACC Cardiovasc Imaging. 2012 September ; 5(9): 941–955. doi:10.1016/j.jcmg.2012.07.007.

Detection of High-Risk Atherosclerotic Plaque:

Report of the NHLBI Working Group on Current Status and Future Directions

Jerome L. Fleg, MD[*], **Gregg W. Stone, MD**[†], **Zahi A. Fayad, PhD**[‡], **Juan F. Granada, MD**[†], **Thomas S. Hatsukami, MD, PhD**[§], **Frank D. Kolodgie, PhD**[‖], **Jacques Ohayon, PhD**[¶], **Roderic Pettigrew, MD, PhD**[¶], **Marc S. Sabatine, MD**[#], **Guillermo Tearney, MD, PhD**[**], **Sergio Waxman, MD**[††], **Michael J. Domanski, MD**[‡], **Pothur R. Srinivas, PhD**[*], and **Jagat Narula, MD, PhD**[‡]

[*]National Heart, Lung and Blood Institute, Bethesda, Maryland [†]Columbia University Medical Center and the Cardiovascular Research Foundation, New York, New York [‡]Mount Sinai School of Medicine, New York, New York [§]University of Washington, Seattle, Washington [‖]Cardiovascular Pathology Institute, Gaithersburg, Maryland [¶]National Institute of Diabetes, Digestive, and Kidney Diseases, Bethesda, Maryland [#]Brigham and Women's Hospital and Harvard Medical School, Boston, Massachusetts [**]Massachusetts General Hospital and Harvard Medical School, Boston, Massachusetts [††]Lahey Clinic, Boston, Massachusetts

Abstract

The leading cause of major morbidity and mortality in most countries around the world is atherosclerotic cardiovascular disease, most commonly caused by thrombotic occlusion of a high-risk coronary plaque resulting in myocardial infarction or cardiac death, or embolization from a high-risk carotid plaque resulting in stroke. The lesions prone to result in such clinical events are termed *vulnerable* or *high-risk plaques*, and their identification may lead to the development of pharmacological and mechanical intervention strategies to prevent such events. Autopsy studies

Reprint requests and correspondence: Dr. Jerome L. Fleg, Division of Cardiovascular Sciences, National Heart, Lung, and Blood Institute, 6701 Rockledge Drive, Room 8150, Bethesda, Maryland 20892. flegj@nhlbi.nih.gov. OR Dr. Jagat Narula narula@mountsinai.org.

CME Editor: Ragavendra R. Baliga, MD

Accreditation and Designation Statement
The American College of Cardiology Foundation (ACCF) is accredited by the Accreditation Council for Continuing Medical Education (ACCME) to provide continuing medical education for physicians.
The ACCF designates this Journal-based CME activity for a maximum of 1 *AMA PRA Category 1 Credit(s)*™. Physicians should only claim credit commensurate with the extent of their participation in the activity.

Method of Participation and Receipt of CME Certificate
To obtain credit for this CME activity, you must:

1. Be an ACC member or *JACC: Cardiovascular Imaging* subscriber.
2. Carefully read the CME-designated article available online and in this issue of the journal.
3. Answer the post-test questions. At least 2 out of the 3 questions provided must be answered correctly to obtain CME credit.
4. Complete a brief evaluation.
5. Claim your CME credit and receive your certificate electronically by following the instructions given at the conclusion of the activity.

CME Editor Disclosure: *JACC: Cardiovascular Imaging* CME Editor Ragavendra R. Baliga, MD, has reported that he has no relationships to disclose.

All other authors have reported that they have no relationships relevant to the contents of this paper to disclose. H. William Strauss, MD, served as Guest Editor for this paper.

from patients dying of acute myocardial infarction or sudden death have shown that such events typically arise from specific types of atherosclerotic plaques, most commonly the thin-cap fibroatheroma. However, the search in human beings for vulnerable plaques before their becoming symptomatic has been elusive. Recently, the PROSPECT (Providing Regional Observations to Study Predictors of Events in the Coronary Tree) study demonstrated that coronary plaques that are likely to cause future cardiac events, regardless of angiographic severity, are characterized by large plaque burden and small lumen area and/or are thin-cap fibroatheromas verified by radiofrequency intravascular ultrasound imaging. This study opened the door to identifying additional invasive and noninvasive imaging modalities that may improve detection of high-risk atherosclerotic lesions and patients. Beyond classic risk factors, novel biomarkers and genetic profiling may identify those patients in whom noninvasive imaging for vulnerable plaque screening, followed by invasive imaging for risk confirmation is warranted, and in whom future pharmacological and/or device-based focal or regional therapies may be applied to improve long-term prognosis.

Keywords

cardiovascular event; high-risk plaque; imaging; prognosis; vulnerable plaque

---

The National Heart, Lung, and Blood Institute (NHLBI) convened a Working Group in Bethesda, Maryland, on June 8, 2009, to examine the current state of the art in the identification of high-risk atherosclerotic plaque and provide recommendations for future research. After discussing the PROSPECT (Providing Regional Observations to Study Predictors of Events in the Coronary Tree) study (1) and related natural history studies, we review the pathological basis for high-risk plaques, invasive and noninvasive plaque imaging modalities, biomarkers that may help to identify high-risk patients, and animal models of coronary atherosclerosis, and conclude with the identification of future research priorities and recommendations.

The Nature and Natural History of Vulnerable Plaque: a Convergence of Understanding

Vulnerable plaque is a term that represents “the susceptibility of a plaque to rupture” (2). From autopsy studies in patients who had died of cardiac causes, the most common underlying plaque morphology was a ruptured thin-cap fibroatheroma (TCFA), with superimposed thrombosis (3). Given this pathophysiological background, the goal emerged to identify such vulnerable plaques in stable patients, with the ultimate goal of preventing plaque rupture, thereby averting myocardial infarction (MI) and sudden cardiac death. It was originally believed that most cases of acute coronary syndrome (ACS) would arise from acute coronary occlusion by severe atherosclerotic plaques. Early prospective angiographic studies, such as the randomized CASS (Coronary Artery Surgery Study) of medical therapy versus coronary artery bypass graft surgery, seemed to support this hypothesis, demonstrating that severely stenotic angiographic lesions were more likely to result in future coronary occlusion and MI than milder stenoses (4). In contrast, retrospective studies reported that the lesions most likely to cause future MI arise from angiographically mild lesions (5). Similarly, a study from the 1997 to 1999 NHLBI Dynamic Registry reported that in 5.8% of 3,747 patients undergoing percutaneous coronary intervention (PCI), clinical progression of coronary artery disease (CAD) (most often ACS) developed within 1 year, requiring an unplanned revascularization procedure. In these patients, the mean angiographic diameter stenosis progressed from 42 ± 21% to 84 ± 14% in a mean of 5.2 months (6). A major limitation of these studies was the reliance on coronary angiography to determine lesion severity and plaque composition.

In contrast to angiography, gray-scale intravascular ultrasound (IVUS) imaging, based on amplitude analysis of sound waves backscattered from tissue, can visualize the external elastic lamina of the vessel wall, allowing determination of vessel size and plaque burden and morphology (7). Radiofrequency (RF) analysis of the ultrasonic signal (virtual histology RF-IVUS) permits further characterization of plaque composition, which correlates well with histological analysis (8). With RF-IVUS, coronary atherosclerotic lesions can be classified into TCFA, thick-cap fibroatheromas, pathological intimal thickening, fibrotic plaque, and fibrocalcific plaque.

In the prospective, multicenter PROSPECT study of patients presenting with ACS, 3-vessel angiography and intracoronary imaging with gray-scale and RF-IVUS were performed to evaluate the characteristics of nonculprit lesions that progress over time to result in major adverse cardiac events (MACE), defined as the composite of cardiac death, cardiac arrest, MI, or unstable/increasing angina requiring rehospitalization (1). In PROSPECT, 697 patients (median age, 58 years; 76% men, 17% with diabetes) presenting with ACS (30% ST-segment elevation MI, 66% non–ST-segment MI, 4% unstable angina) underwent uneventful 1- or 2-vessel PCI followed by quantitative angiography of each millimeter of the entire coronary tree with a diameter ≥1.5 mm. In addition, the proximal 6 to 8 cm of all 3 major coronary arteries were imaged using RF-IVUS. By angiography, 1,814 untreated lesions (i.e., those with a visually estimated diameter stenosis of ≥30%) were prospectively identified in the entire coronary tree, and 3,160 untreated lesions were identified by IVUS, defined as ≥3 consecutive frames with plaque burden ≥40% (7).

Patients were followed prospectively to determine which patient and lesion characteristics would correlate with future events. By 3 years, a new MACE had occurred in 20.4% of patients, nearly equally divided between those caused by untreated nonculprit lesions and those arising from the original ACS culprit lesions that were previously treated by PCI (Fig. 1, top). Most lesions causing nonculprit lesion events arose from angiographically mild (<50%) stenoses; the mean angiographic diameter stenosis of the 106 nonculprit lesions subsequently responsible for MACE increased from 32.3 ± 20.6% at baseline to 65.4 ± 6.3% at follow-up ($p < 0.001$), often with new plaque rupture and/or thrombus. However, likely due to intensive pharmacotherapy and close follow-up, most patients presented with severe progressive or unstable angina, not death or MI, and were effectively treated by revascularization, usually PCI (1).

By multivariable analysis, the only clinical variables independently associated with nonculprit lesion MACE during follow-up were insulin-treated diabetes and previous PCI (1). No angiographic variable was strongly associated with subsequent events. However, significant independent predictors of nonculprit lesion-related MACE (i.e., events arising from those specific untreated lesions) were plaque burden ≥70% (hazard ratio [HR]: 5.03; $p < 0.001$), the presence of a TCFA by RF-IVUS (HR: 3.35; $p < 0.001$), and a minimal lumen area ≤4.0 mm^2 (HR: 3.21, $p = 0.001$). The presence of 2 or 3 of these 3 characteristics identified lesions with a 10% and 18% likelihood, respectively, of an event arising from that site within 3 years (1). Conversely, the 3-year nonculprit lesion–related MACE rate in >1,650 IVUS lesions with none of these 3 characteristics was only 0.3% (Fig. 1, bottom), and no events arose from coronary segments with <40% plaque area.

This prospective study therefore demonstrated that the plaques likely to cause future coronary events are indeed typically severe, either with a large plaque burden and/or a small minimal lumen area (1). The in vivo observation from the PROSPECT study that TCFA identified by RF-IVUS represent the plaque subtype at highest risk to cause future coronary events also confirms the findings from post-mortem pathological studies and validates the

utility of RF-IVUS as an imaging tool capable of identifying vulnerable plaques before they cause subsequent MACE (9).

Pathological Basis for Imaging Vulnerable Plaques

Pathological intimal thickening is the first and most common clinically detectable manifestation of atherosclerosis in humans (10). Unique to these lesions is the presence of lipid pools located in the deeper intima in areas rich in proteoglycans with speckled calcification and a generalized loss of smooth muscle cells. The loss of these cells in lipid pools occurs from cell death, including apoptosis, characterized by prominent basal laminae around clusters of vesicles, consistent with a smooth muscle cell origin (11). The extent of macrophage infiltration is variable and mostly confined to the luminal aspect of the plaque outside the lipid pool. The development of advanced atheromatous plaques with necrotic cores is believed to occur due to invasion of lipid pools by macrophages. Figure 2 demonstrates several important pathological features of atherosclerotic coronary plaques.

Autopsy studies have shown that a ruptured TCFA with overlying thrombus is the most common plaque morphology in the coronary arteries of patients dying of acute MI or sudden cardiac death (3). Thus, the ability of imaging techniques to detect intact TCFA before rupture depends on their ability to detect the typical morphological and biological/functional characteristics of these lesions. By definition, a TCFA contains a large necrotic core of lipid and cellular debris, covered by a thin fibrous cap, usually <65 μm in thickness. The fibrous cap is heavily infiltrated by inflammatory cells and macrophages, indicating the important role of inflammation in plaque instability. Spotty calcifications are often present in the fibrous cap. Neovascularization of the arterial wall, caused by the proliferation of adventitial vasa vasorum in response to hypoxia-induced thickening of the arterial wall, may result in intraplaque hemorrhage. Expansive remodeling of the arterial wall occurs, presumably due to the large plaque burden and limited room for inward growth.

Considering that the necrotic core is a recognized feature of plaque vulnerability, it is particularly important to understand the role of primary and secondary inflammation, cell death, and removal of debris, and other crucial factors that may be involved in the formation of the necrotic core, such as tissue disruption proteases (12) and hemorrhage (13). The free cholesterol content of necrotic cores in high-risk plaques is markedly greater than in lower-risk plaques. Free cholesterol is prominently deposited by the extravasation of erythrocytes from the intimal neovascularization; the new vessels are leaky, and red blood cell membranes are rich in free cholesterol (13). The vulnerable plaque is typically proximal in location, except in the right coronary artery, and more likely to occur near branch points because its occurrence is directed by biomechanical flow disturbances (14). Because only a fraction of vulnerable plaques will likely progress to rupture, and of those that rupture, only a minority will cause a clinical event, the challenge is to identify the unique features critical to this outcome. Various noninvasive imaging techniques may serve as useful screening tools to help identify vulnerable patients and elucidate morphological features of plaques likely to rupture. However, it is likely that confirmation of coronary plaque vulnerability will require intravascular imaging procedures, given their close proximity to the plaque with a higher attendant signal-to-noise ratio, allowing better definition of morphological features associated with future plaque rupture (15).

Intracoronary Imaging Strategies for Confirmation of Plaque Characteristics

IVUS: plaque burden, lipid fibrous content, and remodeling

Although IVUS has been widely used to examine the coronary arterial tree, several recently developed applications of IVUS have helped to detect unstable plaques, including backscatter RF analysis for tissue characterization, elastography, shear stress mapping, vasa vasorum imaging, thermal strain imaging, and measurement of transverse stress tensor (Fig. 3) (16). Some applications such as RF analysis provide information regarding plaque composition, whereas other applications provide functional or physiological data that could be used for mechanistic studies of disease progression. RF ultrasound signals allow identification of different components of atherosclerotic plaques: calcium, fibrous tissue, fibrofatty tissue, and necrotic core (8). Ex vivo validation studies have reported high accuracy for the classification of those plaque signatures. Clinical studies have shown the applicability of RF analysis for characterization of coronary lesions (1,17), as discussed earlier.

Assessment of plaque instability may be enhanced by considering the combination of cap thickness, necrotic core thickness (rather than global size), and the arterial remodeling index (18) (Fig. 4). At the early stages of positive vascular remodeling (PVR), lesions with large relative necrotic cores are biomechanically more prone to rupture, which could explain the progression and growth of clinically silent plaques (18). Although various IVUS methodologies (19–21) provide plaque composition and morphology, biomechanical approaches have been employed to obtain in vivo modulograms (Young's modulus maps) of atheromatous plaques (22) for quantification of stiffness distribution across the plaque (Fig. 3D).

Angioscopy: plaque surface characteristics

Similar to ultrasound, optical characterization of atherosclerotic plaques may provide information about lipid composition of high-risk plaques. Angioscopy has consistently demonstrated an association between yellow plaque color and lipid-rich plaques, including those causing MI (23,24). Angioscopy has also established a link between the presence of yellow plaques and the risk of subsequent coronary events (24). Yellow plaques defined by quantitative colorimetry have been associated with lipid core plaques (LCP) underneath thin fibrous caps and high-risk lesions in patients. Furthermore, certain colorimetric characteristics (including yellow and red colors) may be very sensitive and specific for lipid cores underneath thin fibrous caps. Angioscopy has also identified an association of yellow plaque with delayed and incomplete healing and the presence of thrombus within drug-eluting stents (25).

Near-infrared spectroscopy: lipid core burden

Atherosclerotic plaques, especially lipid-rich plaques, have a specific chemical signature related to cholesterol esters present in lipid cores. Ex vivo studies have demonstrated the feasibility of atherosclerotic lipid-rich plaque detection using near-infrared spectroscopy (NIRS). A catheter-based NIRS system and a chemometric algorithm for the detection of LCP was recently developed and prospectively validated in a human coronary artery autopsy study (26). NIRS data are presented as a "chemogram" representing the probability that an LCP is present (yellow for high probability, red for low probability). LCP was defined as fibroatheroma with a lipid core >60° in circumferential extent and >200 μm in thickness on a cross-sectional histological specimen, with a fibrous cap with a mean thickness ≤450 μm. NIRS identified localized LCP with an area under the receiver-operating characteristic curve

of 0.80 in vessels ≤3.0 mm in diameter. A first-in-human validation study demonstrated the mathematical and statistical similarity of spectra acquired in vivo compared with those obtained in autopsy specimens (Fig. 5) (27); the algorithm identified LCP in 60% of imaged segments in patients undergoing PCI for stable angina or ACS. NIRS can collect data with rapid acquisition times, avoiding the need to obstruct blood flow. A limitation of NIRS, however, is that it does not create an image of the vessel wall. Thus, no information is provided on the depth of LCP. Fibroatheromas that are thick capped or too small to be defined as LCP are major sources of false-positive readings.

Optical coherence tomography: fibrous cap thickness

Optical coherence tomography (OCT), a technique that measures the depth-resolved back-reflection of infrared light, offers high-resolution measurement of fibrous cap thickness, the most important characteristic of high-risk plaque. Newer OCT systems may also define the macrophage density (28) and collagen composition of fibrous caps (29). OCT has an axial (depth) resolution of 5 to 20 μm and a transverse resolution of ~30 μm, which are 10-fold higher than those for IVUS. Imaging depth within the coronary wall ranges from 1 to 3 mm, depending on tissue type. The high resolution of OCT uniquely enables the visualization of microstructural features of coronary plaque types implicated in ACS.

Clinical applicability of OCT was initially limited by attenuation of its optical beam by intraluminal blood, which prevented clear visualization of the vessel wall. Second-generation OCT technologies, including Fourier-domain OCT, have essentially solved this problem by providing imaging at rates 10- to 100-fold faster than first-generation OCT. In combination with a short, nonocclusive saline solution flush and rapid pullback, the faster imaging speed of second-generation OCT technology enables visualization of 3-dimensional microstructure of long coronary artery segments (30) (Fig. 6). OCT can image important plaque characteristics such as rupture, thrombus, thin caps, lipid cores, and calcium. Recent technical advances include increased imaging frame rates (31), improved resolution, and additional contrast mechanisms offered by polarization (collagen) (32), Doppler flow (33), and spectroscopic OCT (34). Multimodal OCT technologies that incorporate molecular probes (35) can provide combinations of structural and molecular imaging. A major limitation of OCT is its lack of penetration. As the external elastic membrane of the entire coronary vessel cannot usually be seen, it is typically not possible with OCT to assess true vessel size and plaque burden. Thus, all imaging modalities have inherent limitations, and comparative natural history studies like the PROSPECT study are required to determine their relative accuracy in predicting future vulnerable plaque-related events.

Intravascular magnetic resonance imaging: plaque composition

Intravascular magnetic resonance imaging (MRI), using pulse field gradient technology has been used to calculate the water diffusion coefficient in atherosclerotic plaques, thereby quantifying their lipid contents using a conventional gray-scale image (36). Preliminary data in human coronary arteries suggest that intravascular MRI can accurately identify the lipid, fibrous, and calcium content of plaque (37). Limitations include the modest spatial resolution (~100 μm) and the need to use an occluding balloon to avoid signal interference from blood.

Noninvasive Characterization of Plaque Morphology

Computed tomography angiography: plaque attenuation and PVR

Computed tomography angiography (CTA) has been predominantly investigated as a less invasive means to detect and quantify arterial lumen narrowing compared with traditional coronary angiography. In addition, CTA has a distinct advantage of simultaneously

demonstrating plaque and necrotic core extent and the type of segmental remodeling (38). CTA of disrupted plaques in patients who experienced ACS (Fig. 7) showed PVR (external vessel wall diameter of ≥110% compared with normal proximal or distal segment) and low-attenuation plaque (LAP) (<30 Hounsfield units) (39).

The 2 CTA features (PVR and LAP) in subjects who have not experienced ACS predict a higher likelihood of plaque rupture over time (39). In a study of >10,000 coronary artery segments from >1,000 patients, individuals with 2-feature positive plaques demonstrated a 22% likelihood of the development of ACS over a 2-year follow-up period compared with <0.5% of those patients whose plaques showed neither PVR nor LAP (39). The greater the remodeling and larger the plaque area, the higher was the likelihood of patients experiencing ACS and the earlier the acute event occurred. The absence of these 2 features excluded the likelihood of an event in more than three-fourths of patients. Patients with no coronary plaques did not experience ACS on follow-up. Positively remodeled lipid-rich plaques may demonstrate delayed contrast enhancement on serial imaging, suggesting the presence of plaque neovascularization (40). Such plaques are also predictive of slow or no-flow outcomes after coronary intervention (41). Interventions with statins cause parallel reductions in overall plaque and LAP volumes and negative plaque remodeling, without significantly influencing the luminal volume (42). Of interest, spotty calcification has been reported to be more commonly associated with culprit lesions, and large calcific plates with stable plaques (42). The detection of activated macrophages using a nanoparticulate computed tomography (CT) contrast agent may allow insights into the biological activity of plaque (43).

The interpretation of such features on CTA, however, is not without limitations. Suboptimal resolution does not allow precise definition of the vascular boundary, and the extent of PVR may be overestimated or underestimated. Similarly, LAP is defined based on the assessment of Hounsfield units, and various imaging or technical parameters may significantly influence the soft plaque measurements. The comparison of IVUS and CTA has demonstrated that the majority of echolucent plaque cores measured <30 Hounsfield units (38). Heavy plaque calcification in some patients may preclude obtaining information about plaque vulnerability. Also, plaque erosions are currently not amenable to CT characterization. CTA is not indicated in the evaluation of most asymptomatic patients given the fear of radiation burden. Primary prevention studies are needed to evaluate the merit of plaque characterization and to define the population that will benefit the most from such a strategy.

MRI: plaque morphology and intraplaque hemorrhage

The superficial location and relative immobility of the carotid artery provide optimal conditions for serial in vivo imaging of human atherosclerosis. Histological studies have shown that many features described in high-risk coronary atherosclerosis are also observed in carotid plaques excised from patients with recent ischemic stroke (44). Patients undergoing carotid endarterectomy provide the unique opportunity to validate in vivo pre-operative imaging of human atherosclerosis by detailed histological analysis of intact excised specimens. MRI can accurately characterize key features of carotid atherosclerosis, including the fibrous cap (45), necrotic core (45), intraplaque hemorrhage (IPH), and mural thrombus (46) (Fig. 8). The rate of diffusion of gadolinium contrast into the carotid vessel wall via dynamic contrast-enhanced MRI allows assessment of plaque macrophage content and degree of plaque neovascularization (47).

A prospective, longitudinal MRI study in 154 asymptomatic patients with 50% to 80% carotid stenosis demonstrated that a thin or ruptured fibrous cap (HR: 17.0; $p < 0.001$), IPH (HR: 5.2; $p = 0.005$), and larger mean necrotic core area (HR: 1.6; $p = 0.01$ per 10-mm^2 increment) were plaque features predictive of subsequent transient ischemic attack or stroke

during a mean follow-up of 3 years (48). Another study of 64 recently symptomatic patients with 30% to 70% carotid stenosis confirmed the critical role of IPH in the development of subsequent transient ischemic attack or stroke (49). IPH was observed in 60% of the ipsilateral carotid arteries on baseline MRI. During a median follow-up of 28 months, 14 ipsilateral ischemic events occurred, 13 of which occurred in carotid arteries with IPH (HR: 9.8; $p = 0.03$). These single-center, prospective studies provide compelling preliminary evidence that specific MRI-identified carotid plaque features are associated with an increased risk of future ischemic events. Larger multicenter studies are needed to confirm these promising initial findings and to determine the plaque features most predictive of future events.

Arteriosclerotic plaque burden in the abdominal aorta can be measured using multicontrast-weighted MRI (50). Studies have demonstrated regression of abdominal aortic plaque burden after intensive statin therapy (51).

Positron emission tomography and molecular imaging: plaque inflammation

Quantifying plaque inflammation may be valuable for several reasons. Pathological studies in patients dying after an ACS event have demonstrated intense inflammation in the culprit plaques, and epidemiological studies have confirmed the association between biomarkers of systemic inflammation and the development of acute coronary events.

Noninvasive quantification of inflammation by molecular imaging has most commonly used single-photon emission CT and positron emission tomography (PET) (52–55). The superior spatial resolution of PET (4 to 5 mm) makes it more attractive than single-photon emission CT (10 to 15 mm). Further, PET modalities demonstrate sensitivity for the detection of molecular targets within the picomolar range, translating into the ability to use small doses of contrast agent compared with MRI and CT. However, the spatial and temporal resolution of MRI and CT are superior to nuclear imaging techniques, and hybrid imaging combining CT or MRI with PET or single-photon emission CT provides the best avenues for molecular imaging. Imaging techniques such as fluorodeoxyglucose (FDG) PET (53), dynamic contrast enhancement MRI (54), and ultrasmall particle iron oxide–enhanced MRI (55) are close to clinical applicability (Table 1). A strong direct correlation between carotid FDG uptake and macrophage density (mean percentage of staining of CD68+ cells) in the carotid endarterectomy specimens has been demonstrated (56), supporting the hypothesis that glucose uptake in atherosclerotic plaques parallels inflammatory activity. FDG uptake did not correlate with plaque area, thickness, or smooth muscle cell prevalence. Serial prospective FDG uptake studies have reported excellent interobserver, intraobserver, and interscan reproducibility.

After anecdotal reports of FDG uptake in coronary arteries (57), a recent prospective FDG PET-CTA study demonstrated the feasibility of FDG localization in inflamed coronary arteries (Fig. 9) (58). In patients who had undergone coronary stent implantation for ACS or chronic stable angina, culprit lesions demonstrated substantially higher FDG uptake compared with stable target lesions. FDG uptake was also prominently present in some nonstented coronary segments, particularly at the left main bifurcation and also in the aortic root (58). Although this study suggests the possibility of plaque characterization for CAD management, it will be necessary to reduce the radiation exposure from combined PET/CT studies. Newer PET tracers that offer promise in detecting increased biological plaque activity include 11C-PK11195 and 18FFEDAA (59), (macrophage infiltration), and ^{68}Ga-DOTATATE (somatostatin receptor analog) (60).

Ultrasound imaging: carotid plaque morphology and neovascularization

B-mode ultrasound with pulse-wave and color Doppler is a convenient noninvasive means to determine the presence and size of plaques in superficial arteries such as the carotid. Plaque can be characterized as homogeneous or heterogeneous. The latter are more likely to be unstable, with a higher potential for embolization or thrombosis (61). Such plaques generally have low calcium content but large amounts of intraplaque hemorrhage and lipid, which make them appear hypoechoic (62). In contrast, calcified (hard) plaque is generally stable and has high echogenicity. Ulcerated plaque may demonstrate eddy flow within the plaque depressions on Doppler or gray-scale flow imaging (63).

Intravenous injection of a contrast agent allows detection of plaque neovascularization, a frequent forerunner of IPH, thus providing additional information to that from standard ultrasound imaging (64). Transesophageal echocardiography has been used to identify ulcerated plaque in the aortic arch and proximal descending aorta, which is associated with increased risk of ischemic stroke (65).

Screening Before Imaging Procedures: Protein and Genetic Biomarkers

Although the development of imaging techniques will remain the cornerstone for the recognition of vulnerable plaques, it is equally important to define a strategy for identifying individuals who will benefit most from these imaging procedures. Circulating biomarkers of inflammation and genetic assessment appear especially promising to identify high-risk patients for potential noninvasive and possibly invasive imaging.

The most widely tested of the inflammatory biomarkers is high-sensitivity C-reactive protein, which has been shown to predict the risk of a first MI in healthy cohorts and future coronary events in patients with stable CAD (66). Whether C-reactive protein is directly causal remains contested, but the association with clinical events remains clear. Multiple other circulating markers hold promise but have not been as widely tested. These include lipoprotein-associated phospholipase A_2 (67), secretory type II phospholipase A_2 (68), oxidized low-density lipoprotein (69), myeloperoxidase (70), and pregnancy-associated plasma protein A (71). In addition to plaque-related circulating markers, several common genetic variants have been reproducibly associated with CAD risk. Each copy of the risk allele at 9p21 increases CAD risk by 25%, and ~50% of individuals of European ancestry harbor at least 1 copy of the risk allele (72). Recently, a multistage genome-wide association study identified 9 genetic variants associated with early-onset MI: 3 of these are newly identified (21q22, 6p24, and 2q33) and 6 (9p21, 1p13, 10q11, 1q41, 19p13, and 1p32) replicated previous observations. To evaluate the cumulative effect of these single-nucleotide polymorphisms on the risk of MI, a genotype score from 9 single-nucleotide polymorphisms was created. Individuals with scores in the top quintile had a >2-fold increase in risk of MI compared with those in the bottom quintile (73).

An important potential use of biomarkers is to guide the use of noninvasive and/or invasive imaging procedures. In 1,004 asymptomatic Korean patients who underwent coronary CTA imaging as part of a health screening, individuals with C-reactive protein ≥2 mg/l had a much higher prevalence of coronary plaque (30.7% vs. 16.7%) and mixed calcific plaque (19.3% vs. 6.3%) compared with those with lower C-reactive protein levels (74).

Animal Models of Unstable Atherosclerotic Plaques

Several animal models of atherosclerosis have been developed for vulnerable plaque research over the past 50 years. The selection of the most appropriate model depends on whether plaque morphology, rupture, or thrombosis is the main objective of the proposed

research. Atherosclerotic lesions, most similar to those in humans, develop in the rhesus monkey (75). Although appealing due to their genetic background and biological similarities to humans, primates have not been widely used because of ethical issues, risk to experimenters, and maintenance costs.

Swine models of atherosclerosis are particularly relevant due to their close anatomic and biological resemblance to the human coronary vasculature (76). The familial hypercholesterolemic swine has severe hypercholesterolemia (>350 mg/dl) even if maintained on a cholesterol-free diet and complex atheromatous lesions develop in 18 months. Eccentric lesions resembling human-like TCFAs develop in this strain of animal. More advanced lesions including large necrotic cores, thinning of the fibrous cap, and IPH are commonly seen in pigs older than 2 years. Similarly, streptozotocin-induced diabetes in swine produces an accelerated form of atherosclerosis, especially when combined with a high cholesterol diet. Atheromatous lesions in this model develop in the first 2 to 3 cm of the proximal arteries as early as 20 weeks after the induction of diabetes. In addition, their well-described genetic background, as well as their vascular response to therapies, makes these models suitable for research in which a well-defined coronary territory is required. The atherosclerotic rabbit is a cost-effective model of atherosclerosis if the coronary territory is not a specific target of the proposed research. Although the morphology of the lesions differs from late-stage human atherosclerosis, macrophage foam cell–rich atherosclerotic plaques develop relatively rapidly in cholesterol-fed rabbits (77). The development period of these lesions can be shortened by inducing initial endothelial injury or by intramural injection of proatherosclerotic material such as red blood cell membranes.

Previously healed ruptures are commonly found in porcine atherosclerotic models and less commonly in rabbits. In small animal models, particularly genetically manipulated mice, complex atheromas usually develop after cholesterol diet supplementation and frequently atypically ruptured lesions in the innominate artery develop. In such models, a combination of dietary manipulation and the application of mechanical obstructions such as cuffs have shortened the development time and increased the reproducibility, complexity, and likelihood of rupture of the induced lesions (78).

Innovative imaging detection and therapeutic technologies will ultimately depend on developing successful animal models and standardizing lesion definitions, permitting preclinical validation of the technology in a controlled environment. The morphological features and clinical utility of various animal models of atherosclerosis are shown in Table 2.

Broad Recommendations From the Working Group

1. **Identifying vulnerable plaques and defining their natural history.** For noninvasive imaging techniques to find clinical application, they must identify high-risk subjects with several-fold better predictive value than currently available clinical approaches. Invasive techniques will need at least 2-fold better predictive power than noninvasive techniques for clinical utility. PROSPECT-type studies are necessary to demonstrate that high-risk lesions identified by either noninvasive or invasive imaging are the focal cause of future MACE (i.e., due to plaque rupture and/or thrombosis) and/or correlate with imaging tools previously validated to predict clinical events (which at present has only been proven for RF-IVUS).
2. **Developing effective preventive strategies**. After vulnerable plaques (and vulnerable patients) are identified, pharmaceutical and/or device-based interventional tools are needed that may delay or obviate an ominous course for these high-risk plaques and patients.

3. **Determining cost-effectiveness of diagnostic and therapeutic approaches.** Cost-effectiveness studies are mandatory to define the optimal populations and strategies for noninvasive screening, invasive imaging, and potential management of high-risk plaques and patients. It is likely that a combination of selected risk factors, biomarkers, and noninvasive imaging in high-risk populations will best determine who should undergo invasive imaging.

Recommendations for Future Research

1. **Improve understanding of the plaque microenvironment in the pathogenesis of plaque instability.** Examples of possible research proposals include inflammation and immune cell responses, the role of neovascularization and intraplaque hemorrhage, and the role of extracellular matrix composition and biomechanical stress.
2. **Develop and validate molecular and genetic markers of vulnerable plaque.** Examples of possible research proposals include the use of biomarkers to elucidate pathological processes underlying stable and unstable plaques; the use of biomarkers and blood coagulation markers to predict the risk of plaque progression, rupture, or erosion; and the use of biomarkers to assess response to intervention.
3. **Develop and validate noninvasive and invasive imaging techniques to identify, monitor, and treat vulnerable plaques.** Examples of possible research proposals include animal studies to validate promising imaging techniques and molecular markers, with histology both before and after intervention; standardization of acquisition and interpretation of promising imaging techniques; small natural history studies and response to pharmacological or catheter-based interventions in humans using single- or dual-imaging techniques; and large natural history studies and phase 2 treatment trials evaluating the response to pharmacological or catheter-based interventions in humans using single- or multiple-imaging techniques. When possible, such investigations should be leveraged to existing studies to maximize cost-effectiveness.

Acknowledgments

Dr. Stone has been a consultant to InfraReDx, Boston Scientific, Abbott Vascular, Medtronic, and Volcano. Dr. Sabatine has received research grant support (>$25,000) through Brigham and Women's Hospital from Abbott Laboratories, Amgen, AstraZeneca, BRAHMS, Bristol-Myers Squibb/Sanofi-Aventis Joint Venture, Critical Diagnostics, Daiichi-Sankyo, Merck, Roche Diagnostics, and Takeda; has served on the scientific advisory board (< $10,000) for Bristol-Myers Squibb/Sanofi-Aventis Joint Venture, GlaxoSmithKline, Merck, and Pfizer; and (> $10,000) Sanofi-Aventis; and has received research support (>$25,000) from Nanosphere. Dr. Tearney has been a consultant to Samsung and Merck; has performed sponsored research for Terumo Corporation; and has the right to receive royalties from Terumo Corporation and MIT. Dr. Narula serves on the advisory boards of GE, Philips, and Siemens Healthcare.

ABBREVIATIONS AND ACRONYMS

ACS	acute coronary syndrome
CAD	coronary artery disease
CT	computed tomography
CTA	computed tomography angiography
FDG	fluorodeoxyglucose
HR	hazard ratio

IPH	intraplaque hemorrhage
IVUS	intravascular ultrasound
LAP	low-attenuation plaque
LCP	lipid core plaque
MACE	major adverse cardiac event(s)
MI	myocardial infarction
MRI	magnetic resonance imaging
NIRS	near-infrared spectroscopy
OCT	optical coherence tomography
PCI	percutaneous coronary intervention
PET	positron emission tomography
PVR	positive vascular remodeling
RF	radiofrequency
TCFA	thin-cap fibroatheroma

REFERENCES

1. Stone GW, Maehara A, Lansky AJ, et al. A prospective natural-history study of coronary atherosclerosis. N Engl J Med. 2011; 364:226–235. [PubMed: 21247313]
2. Muller JE, Tofler GH, Stone PH. Circadian variation and triggers of onset of acute cardiovascular disease. Circulation. 1989; 79:733–743. [PubMed: 2647318]
3. Virmani R, Burke AP, Farb A, Kolodgie FD. Pathology of the vulnerable plaque. J Am Cardiol. 2006; 47(Suppl 8):C13–C18.
4. Ellis SG, Alderman E, Cain K, Fisher L, Sanders W, Bourassa M. the CASS Investigators. Risk of anterior myocardial infarction by lesion severity and measurement method of stenoses in the left anterior descending coronary distribution: a CASS registry study. J Am Coll Cardiol. 1988; 11:908–916. [PubMed: 3128587]
5. Ambrose JA, Tannenbaum MA, Alexopoulos D, et al. Angiographic progression of coronary artery disease and the development of myocardial infarction. J Am Coll Cardiol. 1988; 12:56–62. [PubMed: 3379219]
6. Glaser R, Selzer F, Faxon DP, et al. Clinical progression of incidental, asymptomatic lesions discovered during culprit vessel coronary intervention. Circulation. 2005; 111:143–149. [PubMed: 15623544]
7. Mintz GS, Nissen SE, Anderson WD, et al. American College of Cardiology clinical expert consensus document on standards for acquisition, measurement, and reporting of intravascular ultrasound studies (IVUS). A report of the American College of Cardiology Task Force on Clinical Expert Consensus Documents. J Am Coll Cardiol. 2001; 37:1478–1492. [PubMed: 11300468]
8. Garcia-Garcia HM, Mintz GS, Lerman A, et al. Tissue characterization using radiofrequency data analysis: recommendations for acquisition, analysis, interpretation and reporting. EuroIntervention. 2009; 5:177–189. [PubMed: 20449928]
9. Stone GW, Maehara A, Mintz GS. The reality of vulnerable plaque detection. J Am Coll Cardiol Img. 2011; 4:902–904.
10. Kolodgie FD, Burke AP, Nakazawa G, Virmani R. Is pathologic intimal thickening the key to understanding early plaque progression in human atherosclerotic disease? Arterioscler Thromb Vasc Biol. 2007; 27:986–989. [PubMed: 17442894]

11. Kockx MM, De Meyer GR, Muhring J, Jacob W, Bult H, Herman AG. Apoptosis and related proteins in different stages of human atherosclerotic plaques. Circulation. 1998; 97:2307–2315. [PubMed: 9639374]
12. Newby AC. Metalloproteinase expression in monocytes and macrophages and its relationship to atherosclerotic plaque instability. Arterioscler Thromb Vasc Biol. 2008; 28:2108–2114. [PubMed: 18772495]
13. Kolodgie FD, Gold HK, Burke AP, et al. Intraplaque hemorrhage and progression of coronary atheroma. N Engl J Med. 2003; 349:2316–2325. [PubMed: 14668457]
14. Stone PH, Coskun AU, Kinlay S, et al. Effect of endothelial shear stress on the progression of coronary artery disease, vascular remodeling, and in-stent restenosis in humans: in vivo 6-month follow-up study. Circulation. 2003; 108:438–444. [PubMed: 12860915]
15. Braunwald E. Epilogue: what do clinicians expect from imagers? J Am Coll Cardiol. 2006; 47:101–103.
16. DeMaria AN, Narula J, Mahmud E, Tsimikas S. Imaging vulnerable plaque by ultrasound. J Am Coll Cardiol. 2006; 18 Suppl 8(47):C32–C39. [PubMed: 16631508]
17. Rodriguez-Granillo GA, Garcia-Garcia HM, McFadden EP, et al. In vivo intravascular ultrasound-derived thin-cap fibroatheroma detection using ultrasound radiofrequency data analysis. J Am Coll Cardiol. 2005; 46:2038–2042. [PubMed: 16325038]
18. Ohayon J, Finet G, Gharib AM, et al. Necrotic core thickness and positive arterial remodeling index: emergent biomechanical factors for evaluating the risk of plaque rupture. Am J Physiol Heart Circ Physiol. 2008; 295:H717–H727. [PubMed: 18586893]
19. Missel E, Mintz GS, Carlier SG, et al. In vivo virtual histology intravascular ultrasound correlates of risk factors for sudden coronary death in men: results from the prospective, multi-centre virtual histology intravascular ultrasound registry. Eur Heart J. 2008; 29:2141–2147. [PubMed: 18596073]
20. Maurice RL, Fromageau J, Cardinal MH, et al. Characterization of atherosclerotic plaques and mural thrombi with intravascular ultrasound elastography: a potential method evaluated in an aortic rabbit model and a human coronary artery. IEEE Trans Inf Technol Biomed. 2008; 12:290–298. [PubMed: 18693496]
21. Schaar JA, van der Steen AF, Mastik F, Baldewsing RA, Serruys PW. Intravascular palpography for vulnerable plaque assessment. J Am Coll Cardiol. 2006; 47:C86–C91. [PubMed: 16631515]
22. Le Floc'h S, Ohayon J, Tracqui P, et al. Vulnerable atherosclerotic plaque elasticity reconstruction based on a segmentation-driven optimization procedure using strain measurements: theoretical framework. IEEE Trans Med Imaging. 2009; 28:1126–1137. [PubMed: 19164080]
23. Ishibashi F, Aziz K, Abela GS, Waxman S. Update on coronary angioscopy: review of a 20 year experience and potential application for detection of vulnerable plaque. J Interv Cardiol. 2006; 19:17–25. [PubMed: 16483335]
24. Ohtani T, Ueda Y, Mizote I, et al. Number of yellow plaques detected in a coronary artery is associated with future risk of acute coronary syndrome: detection of vulnerable patients by angioscopy. J Am Coll Cardiol. 2006; 47:2194–2200. [PubMed: 16750684]
25. Oyabu J, Ueda Y, Ogasawara N, Okada K, Hirayama A, Kodama K. Angioscopic evaluation of neointima coverage: sirolimus drug-eluting stent versus bare metal stent. Am Heart J. 2006; 152:1168–1174. [PubMed: 17161071]
26. Gardner CM, Tan H, Hull EL, et al. Detection of lipid core coronary plaques in autopsy specimens with a novel catheter-based near infrared spectroscopy system. J Am Coll Cardiol Img. 2008; 1:638–648.
27. Waxman S, Dixon SR, L'Allier PL, et al. In vivo validation of a catheter-based near-infrared spectroscopy system for detection of lipid core coronary plaques: initial results and exploratory analysis of the SPECTroscopic Assessment of Coronary Lipid (SPECTACL) multicenter study. J Am Coll Cardiol Img. 2009; 2:858–868.
28. Tearney GJ, Yabushita H, Houser SL, et al. Quantification of macrophage content in atherosclerotic plaques by optical coherence tomography. Circulation. 2003; 107:113–119. [PubMed: 12515752]

29. Nadkarni SK, Pierce MC, Park BH, et al. Measurement of collagen and smooth muscle cell content in atherosclerotic plaques using polarization-sensitive optical coherence tomography. J Am Coll Cardiol. 2007; 49:1474–1481. [PubMed: 17397678]
30. Tearney GJ, Waxman S, Shishkov MS, et al. Three-dimensional coronary artery microscopy by intracoronary optical frequency domain imaging: first-in-human experience. J Am Coll Cardiol Img. 2008; 1:752–761.
31. Oh WY, Yun SH, Tearney GJ, Bouma BE. 115 kHz tuning repetition rate ultrahigh-speed wavelength-swept semiconductor laser. Opt Lett. 2005; 30:3159–3161. [PubMed: 16350273]
32. Giattina SD, Courtney BK, Herz PR, et al. Assessment of coronary plaque collagen with polarization sensitive optical coherence tomography (PSOCT). Int J Cardiol. 2006; 107:400–409. [PubMed: 16434114]
33. Vakoc BJ, Tearney GJ, Bouma BE. Statistical properties of phase-decorrelation in phase-resolved Doppler optical coherence tomography. IEEE Trans Med Imaging. 2009; 28:814–821. [PubMed: 19164078]
34. Xu C, Vinegoni C, Ralston TS, Luo W, Tan W, Boppart SA. Spectroscopic spectral-domain optical coherence microscopy. Opt Lett. 2006; 31:1079–1081. [PubMed: 16625909]
35. Hariri LP, Tumlinson AR, Besselsen DG, Utzinger U, Gerner EW, Barton JK. Endoscopic optical coherence tomography and laser-induced fluorescence spectroscopy in a murine colon cancer model. Lasers Surg Med. 2006; 38:305–313. [PubMed: 16596657]
36. Ferrari VA, Wilensky RL. Intravascular magnetic resonance imaging. Top Magn Reson Imaging. 2007; 18:401–408. [PubMed: 18025994]
37. Regar E, Hennen B, Grube E, et al. First in man application of a miniature self-contained intracoronary magnetic resonance imaging probe. A Multi- Center Safety and Feasibility Trial. EuroIntervention. 2006; 2:77–93. [PubMed: 19755240]
38. Motoyama S, Kondo T, Anno H, et al. Multi-slice compute tomographic characteristics of coronary lesions in acute coronary syndromes. J Am Coll Cardiol. 2007; 50:319–326. [PubMed: 17659199]
39. Motoyama S, Sarai M, Harigaya H, et al. Computed tomographic angiography characteristics of atherosclerotic plaques subsequently resulting in acute coronary syndrome. J Am Coll Cardiol. 2009; 54:49–57. [PubMed: 19555840]
40. Fujimoto S, Kondo T, Kodama T, Takase S, Narula J. Delayed plaque enhancement by coronary CT angiography. J Am Coll Cardiol Img. 2012 In press.
41. Kodama T, Kondo T, Oida A, Fujimoto S, Narula J. Computed tomographic angiography-verified plaque characteristics and slow-flow phenomenon during percutaneous coronary intervention. J Am Coll Cardiol Intv. 2012; 5:636–643.
42. Inoue K, Motoyama S, Sarai M, et al. Serial coronary CT angiography-verified changes in plaque characteristics as an end-point: evaluation of effect of statin intervention. J Am Coll Cardiol Img. 2010; 3:691–698.
43. Hyafil F, Cornily J-C, Feig JE, et al. Noninvasive detection of macrophages using a nanoparticulate contrast agent for computed tomography. Nat Med. 2007; 13:636–641. [PubMed: 17417649]
44. Redgrave JN, Lovett JK, Gallagher PJ, Rothwell PM. Histological assessment of 526 symptomatic carotid plaques in relation to the nature and timing of ischemic symptoms: the Oxford plaque study. Circulation. 2006; 113:2320–2328. [PubMed: 16651471]
45. Cai J, Hatsukami TS, Ferguson MS, et al. In vivo quantitative measurement of intact fibrous cap and lipid-rich necrotic core size in atherosclerotic carotid plaque: comparison of high-resolution, contrast-enhanced magnetic resonance imaging and histology. Circulation. 2005; 112:3437–3444. [PubMed: 16301346]
46. Kampschulte A, Ferguson MS, Kerwin WS, et al. Differentiation of intraplaque versus juxtaluminal hemorrhage/thrombus in advanced human carotid atherosclerotic lesions by in vivo magnetic resonance imaging. Circulation. 2004; 110:3239–3244. [PubMed: 15533871]
47. Kerwin WS, O'Brien KD, Ferguson MS, Polissar N, Hatsukami TS, Yuan C. Inflammation in carotid atherosclerotic plaque: a dynamic contrast-enhanced MR imaging study. Radiology. 2006; 241:459–468. [PubMed: 16966482]

48. Takaya N, Yuan C, Chu B, et al. Association between carotid plaque characteristics and subsequent ischemic cerebrovascular events: a prospective assessment with MRI—initial results. Stroke. 2006; 37:818–823. [PubMed: 16469957]
49. Altaf N, Beech A, Goode SD, et al. Carotid intraplaque hemorrhage detected by magnetic resonance imaging predicts embolization during carotid endarterectomy. J Vasc Surg. 2007; 46:31–36. [PubMed: 17543492]
50. Buhk JH, Finck-Wedel A-K, Buchert R, et al. Screening for atherosclerotic plaques in the abdominal aorta in high-risk patients with multicontrast MRI: a prospective study at 3.0 and 1.5 tesla. Br J Radiol. 2011; 84:883–889. [PubMed: 21081571]
51. Lima JA, Desai MY, Steen H, Warren WP, Gautam S, Lai S. Statin-induced cholesterol lowering and plaque regression after 6 months of magnetic resonance imaging-monitored therapy. Circulation. 2004; 110:2336–2341. [PubMed: 15477398]
52. Sanz J, Fayad ZA. Imaging of atherosclerotic cardiovascular disease. Nature. 2008; 451:953–957. [PubMed: 18288186]
53. Rudd JH, Hyafil F, Fayad ZA. Inflammation imaging in atherosclerosis. Arterioscler Thromb Vasc Biol. 2009; 29:1009–1016. [PubMed: 19304673]
54. Kerwin WS, Oikawa M, Yuan C, Jarvik GP, Hatsukami TS. MR imaging of adventitial vasa vasorum in carotid atherosclerosis. Magn Reson Med. 2008; 59:507–514. [PubMed: 18306402]
55. Tang TY, Howarth SP, Miller SR, et al. The ATHEROMA (Atorvastatin Therapy: Effects on Reduction of Macrophage Activity) study. Evaluation using ultrasmall superparamagnetic iron oxide-enhanced magnetic resonance imaging in carotid disease. J Am Coll Cardiol. 2009; 53:2039–2050. [PubMed: 19477353]
56. Tawakol A, Migrino RQ, Bashian GG, et al. In vivo ^{18}F-fluorodeoxyglucose positron emission tomography imaging provides a noninvasive measure of carotid plaque inflammation in patients. J Am Coll Cardiol. 2006; 48:1818–1824. [PubMed: 17084256]
57. Alexanderson E, Slomka P, Cheng V, et al. Fusion of positron emission tomography and coronary computed tomographic angiography identifies fluorine 18 fluorodeoxyglucose uptake in the left main coronary artery soft plaque. J Nucl Cardiol. 2008; 15:841–843. [PubMed: 18984461]
58. Rogers IS, Nasir K, Figueroa AL, et al. Feasibility of FDG imaging of the coronary arteries: comparison between acute coronary syndrome and stable angina. J Am Coll Cardiol Img. 2010; 3:388–397.
59. Gaemperli O, Shalhoub J, Owen DR, et al. Imaging intraplaque inflammation in carotid atherosclerosis with 11C-PK11195 positron emission tomography/ computed tomography. Eur Heart J. 2012; 33:1902–1910. [PubMed: 21933781]
60. Romiger A, Tobias S, Vogl E, et al. In vivo imaging of macrophage activity in the coronary arteries using 68Ga- DOTATATE PET/CT: correlation with coronary calcium burden and risk factors. J Nucl Med. 2010; 51:193–197. [PubMed: 20080898]
61. Tahmasebpour HR, Buckley AR, Cooperberg PL, Fix CH. Sonographic examination of the carotid arteries. Radiographics. 2005; 25:1561–1575. [PubMed: 16284135]
62. Polak JF, Shemanski L, O'Leary DH, et al. Hypoechoic plaque at US of the carotid artery: an incident risk factor for incident stroke in adults aged 65 years or older. Radiology. 1998; 208:649–654. [PubMed: 9722841]
63. Furst H, Hart WH, Jansen I, et al. Color flow Doppler sonography in the identification of ulcerative plaques in patients with high-grade carotid artery stenosis. Am J Neuroradiol. 1992; 13:1581–1587. [PubMed: 1442434]
64. Xiong L, Deng YB, Zhu Y, Liu YN, Bi XJ. Correlation of carotid plaque neovascularization detected by using contrast-enhanced US with clinical symptoms. Radiology. 2009; 251:583–589. [PubMed: 19304920]
65. Harloff A, Simon J, Brendecke S, et al. Complex plaques in the proximal descending aorta: an underestimated embolic source of stroke. Stroke. 2010; 41:1145–1150. [PubMed: 20431080]
66. Sabatine MS, Morrow DA, Jablonski KA, et al. Prognostic significance of the Centers for Disease Control/ American Heart Association high-sensitivity C-reactive protein cut points for cardiovascular and other outcomes in patients with stable coronary artery disease. Circulation. 2007; 115:1528–1536. [PubMed: 17372173]

67. Sabatine MS, Morrow DA, O'Donoghue M, et al. Prognostic utility of lipoprotein-associated phospholipase A2 for cardiovascular outcomes in patients with stable coronary artery disease. Arterioscler Thromb Vasc Biol. 2007; 27:2463–2469. [PubMed: 17766330]
68. Kugiyama K, Ota Y, Takazoe K, et al. Circulating levels of secretory type II phospholipase A(2) predict coronary events in patients with coronary artery disease. Circulation. 1999; 100:1280–1284. [PubMed: 10491371]
69. Meisinger C, Baumert J, Khuseyinova N, Loewel H, Koenig W. Plasma oxidized low-density lipoprotein, a strong predictor for acute coronary heart disease events in apparently healthy, middle-aged men from the general population. Circulation. 2005; 112:651–657. [PubMed: 16043640]
70. Meuwese MC, Stroes ES, Hazen SL, et al. Serum myeloperoxidase levels are associated with the future risk of coronary artery disease in apparently healthy individuals: the EPIC-Norfolk Prospective Population Study. J Am Coll Cardiol. 2007; 50:159–165. [PubMed: 17616301]
71. Elesber AA, Conover CA, Denktas AE, et al. Prognostic value of circulating pregnancy-associated plasma protein levels in patients with chronic stable angina. Eur Heart J. 2006; 27:1678–1684. [PubMed: 16717071]
72. Samani NJ, Erdmann J, Hall AS, et al. Genome-wide association analysis of coronary artery disease. N Engl J Med. 2007; 357:443–453. [PubMed: 17634449]
73. Kathiresan S, Voight BF, Purcell S, et al. Genome-wide association of early-onset myocardial infarction with single nucleotide polymorphisms and copy number variants. Nat Genet. 2009; 41:334–341. [PubMed: 19198609]
74. Rubin J, Chang H-J, Nasir K, et al. Association between high-sensitivity C-reactive protein and coronary plaque subtypes assessed by 64-slice coronary computed tomography angiography in an asymptomatic population. Circ Cardiovasc Imaging. 2011; 4:201–209. [PubMed: 21422167]
75. Kusumi Y, Scanu AM, McGill HC, Wissler RW. Atherosclerosis in a rhesus monkey with genetic hypercholelesterolemia and elevated plasma Lp(a). Atherosclerosis. 1993; 99:165–174. [PubMed: 8503945]
76. Granada JF, Kaluza GL, Wilensky RL, Biedermann BC, Schwartz RS, Falk E. Porcine models of coronary atherosclerosis and vulnerable plaque for imaging and interventional research. EuroIntervention. 2009; 5:140–148. [PubMed: 19577996]
77. Kolodgie FD, Katocs AS Jr, Largis EE, et al. Hypercholesterolemia in the rabbit induced by feeding graded amounts of low-level cholesterol. Methodological considerations regarding individual variability in response to dietary cholesterol and development of lesion type. Arterioscler Thromb Vasc Biol. 1996; 16:1454–1464. [PubMed: 8977449]
78. Schwartz SM, Galis Z, Rosenfeld ME, Falk E. Plaque rupture in humans and mice. Arterioscler Thromb Vasc Biol. 2007; 27:705–713. [PubMed: 17332493]

CME Objective for This Article

At the end of this activity the reader should be able to discuss: 1) the significance of the vulnerable plaque, particularly thin-cap fibroatheroma, in the pathogenesis of acute myocardial infarction; 2) the role of invasive and noninvasive imaging modalities in the detection of high risk coronary lesions and high risk patients; 3) the utility of novel biomarkers and genetic profiling in the identification of patients who are most likely to benefit from noninvasive imaging for vulnerable plaques, and from invasive imaging for risk confirmation; and 4) the future role of imaging and biomarkers in determining appropriate pharmacologic and/or device based focal or regional therapies.

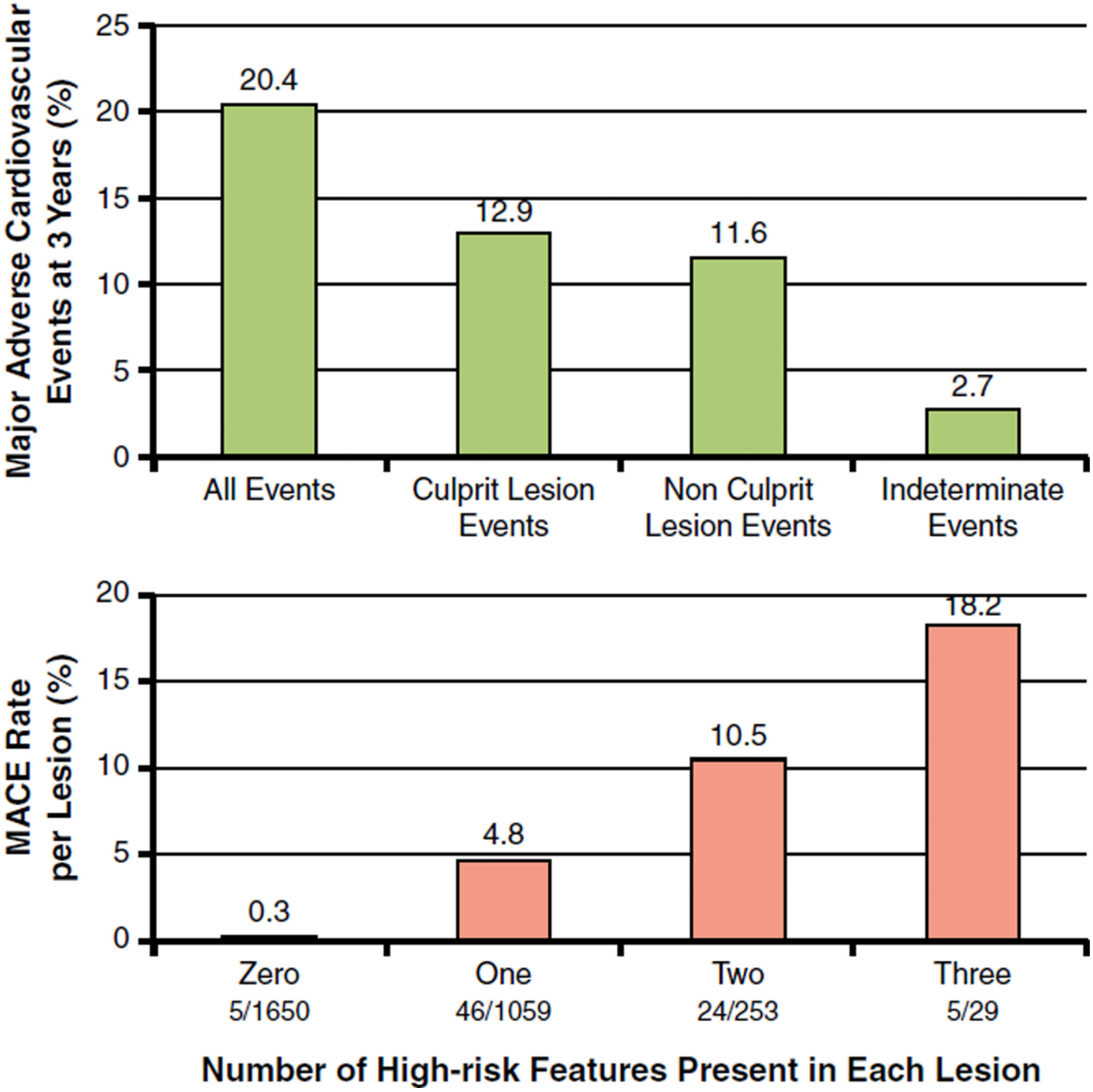

Figure 1. Natural History of Coronary Artery Lesions in ACS: The PROSPECT Study

(Top) Natural history of treated and untreated coronary artery lesions in patients with acute coronary syndromes. Incidence of major adverse cardiac events (MACE) (cardiac death, cardiac arrest, myocardial infarction, or rehospitalization due to unstable or progressive angina) at 3 years after successful percutaneous coronary intervention (PCI) for acute coronary syndrome in 697 patients from the PROSPECT study. Among the 20.4% of patients experiencing events, lesions originally treated by PCI (culprit lesions) and untreated (nonculprit) lesions accounted for nearly equal numbers of events. A small proportion of events were of indeterminate lesion origin because coronary angiography was not performed at the time of the event. **(Bottom)** The rate of MACE per lesion during median follow-up of

3.4 years according to the number of high-risk PROSPECT lesion characteristics at baseline. The high-risk characteristics are a plaque burden ≥70%, a minimal lumen area ≤4.0 mm^2, and a thin-cap fibroatheroma as assessed by virtual histology intravascular ultrasound. The fraction below the x-axis is the number of candidate lesions with each combination of events (denominator) and the number of those lesions that resulted in a MACE event during follow-up (numerator). Adapted, with permission, from Stone et al. (1).

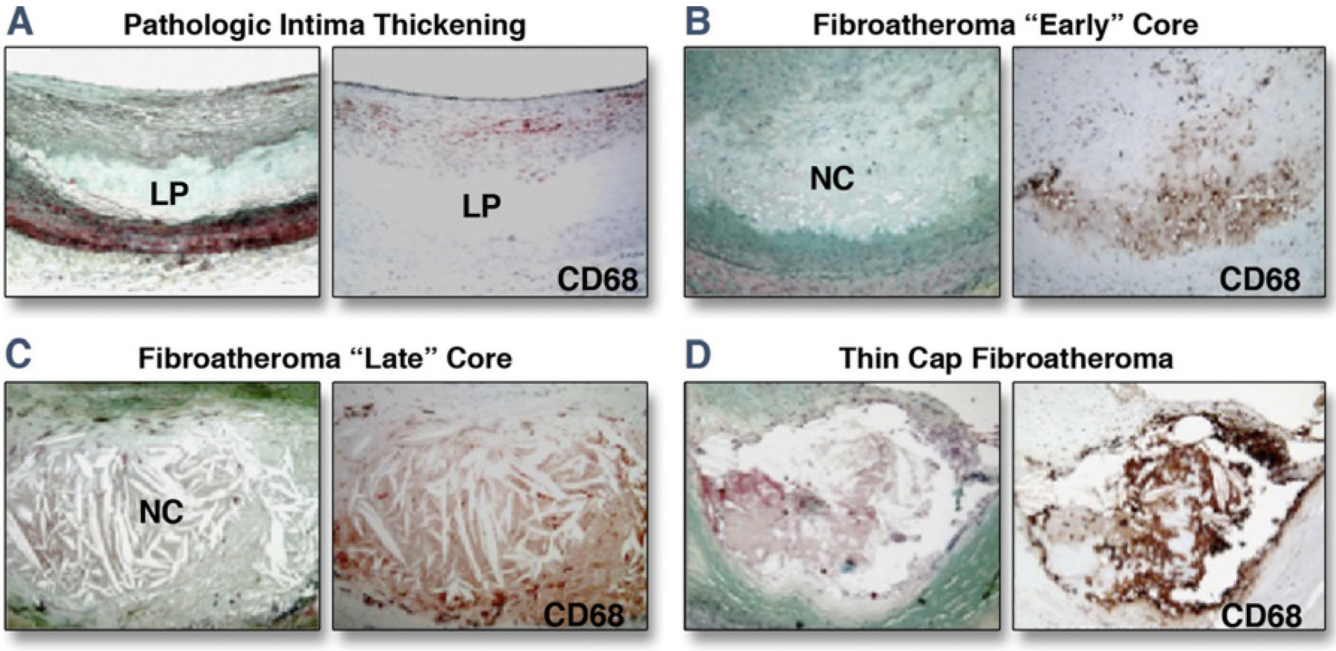

Figure 2. Representative Lesion Morphologies for Progressive Human Coronary Atherosclerosis

(A) The earliest atherosclerotic lesion, pathological intimal thickening, highlighted by lipid pools (LP) in the deep intima (Movat pentachrome stain) with CD68+ macrophages near the luminal surface. **(B)** Fibroatheroma with early necrosis, showing the conversion of a lipid pool into a necrotic core; note the invasion of the lipid pool by macrophages. **(C)** A late core fibroatheroma, distinguished by its lytic environment and increase in size. **(D)** An advanced thin-cap fibroatheroma (rupture-prone lesion), characterized by a relatively large necrotic core and thin fibrous cap infiltrated by macrophages. NC = necrotic core. Adapted, with permission, from Virmani R, Burke AP, Farb A, Gold HK, Finn AV, Kolodgie FD. Plaque rupture. In: Virmani R, Narula J, Leon M, Willerson J, editors. The Vulnerable Atherosclerotic Plaque: Strategies for Diagnosis and Management. Malden, MA: Blackwell Futura, 2007:37–59.

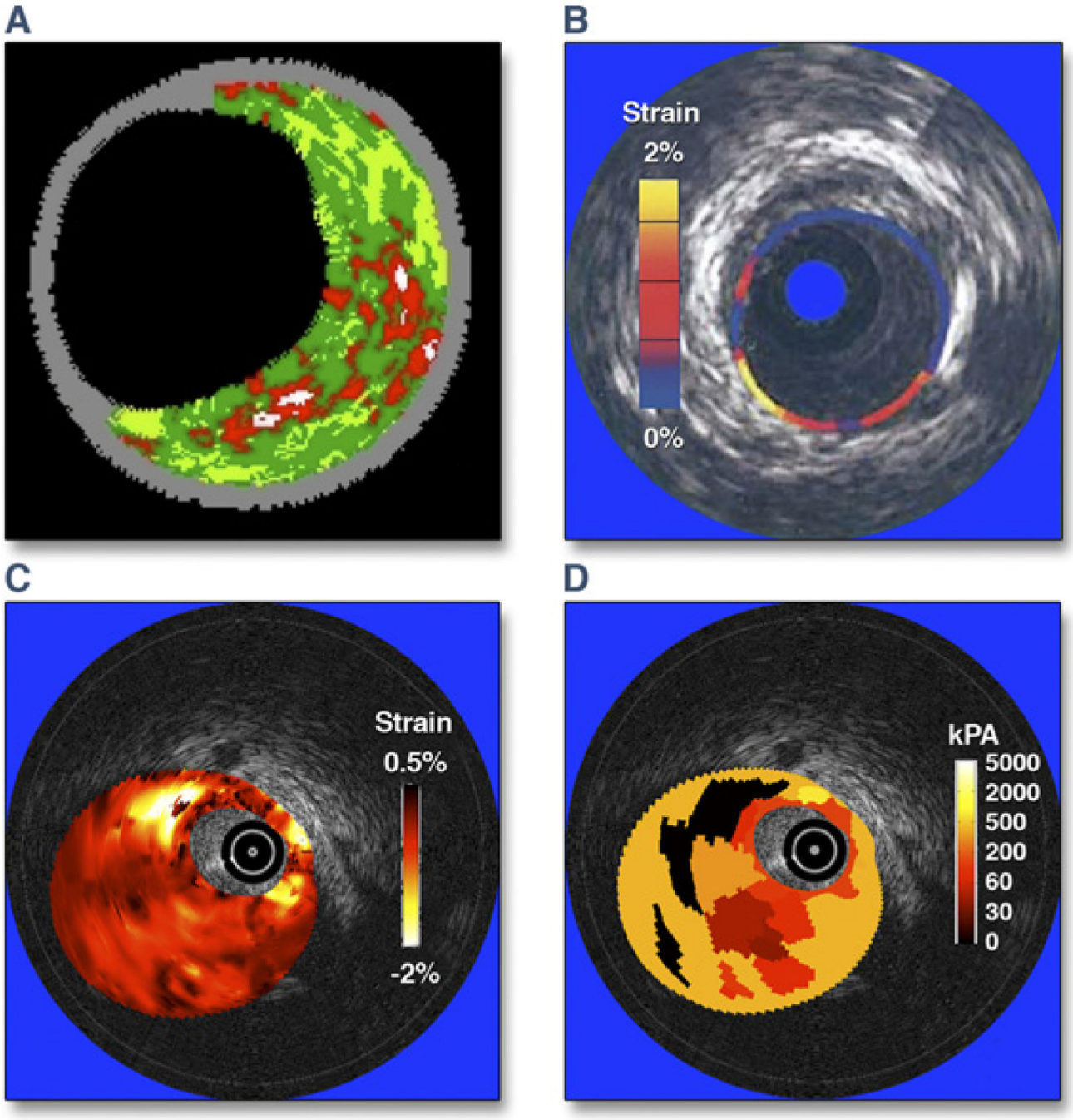

Figure 3. Various Intravascular Ultrasound Imaging Modalities to Assess Coronary Plaques

(A) Plaque composition (virtual histology); courtesy of G. Finet. **(B)** Palpography; reprinted with permission from Schaar et al. (21). **(C)** Strain map (or elastogram); reprinted, with permission, from Le Floc'h et al. (22). **(D)** Elasticity map (or modulogram); reprinted, with permission, from Maurice et al. (20). The elastogram and modulogram in **C** and **D** were obtained from the same vulnerable plaque.

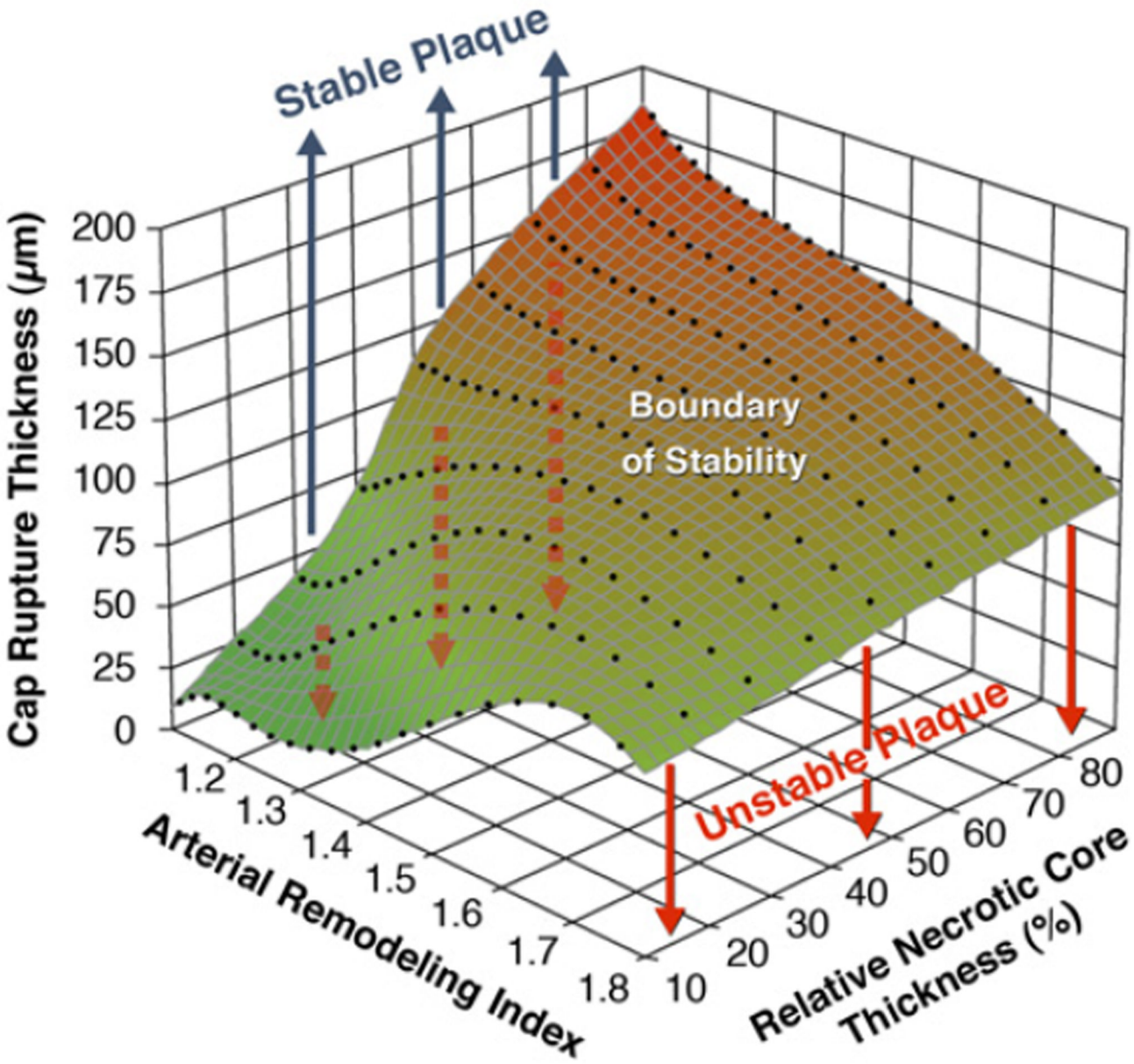

Figure 4. Graph Highlighting the Influences of Remodeling Index and Relative Necrotic Core Thickness on Critical TCFA Thickness

The critical thin-cap fibroatheroma (TCFA) thickness is defined as the value at which cap stress reaches the critical or rupture point tensile stress. Vulnerable plaques with relative necrotic core thicknesses of 90%, 70%, 50%, 30%, and 10% become unstable below their respective curves. Thus, the unstable region for vulnerable plaques with relative necrotic core thickness of 10% is indicated in light gray, whereas for 30% thickness, the unstable region is the summation of gray and green light areas. Plaques with low remodeling index and a large relative necrotic core thickness are more prone to rupture, having a higher critical TCFA thickness. Reprinted, with permission, from Ohayon et al. (18).

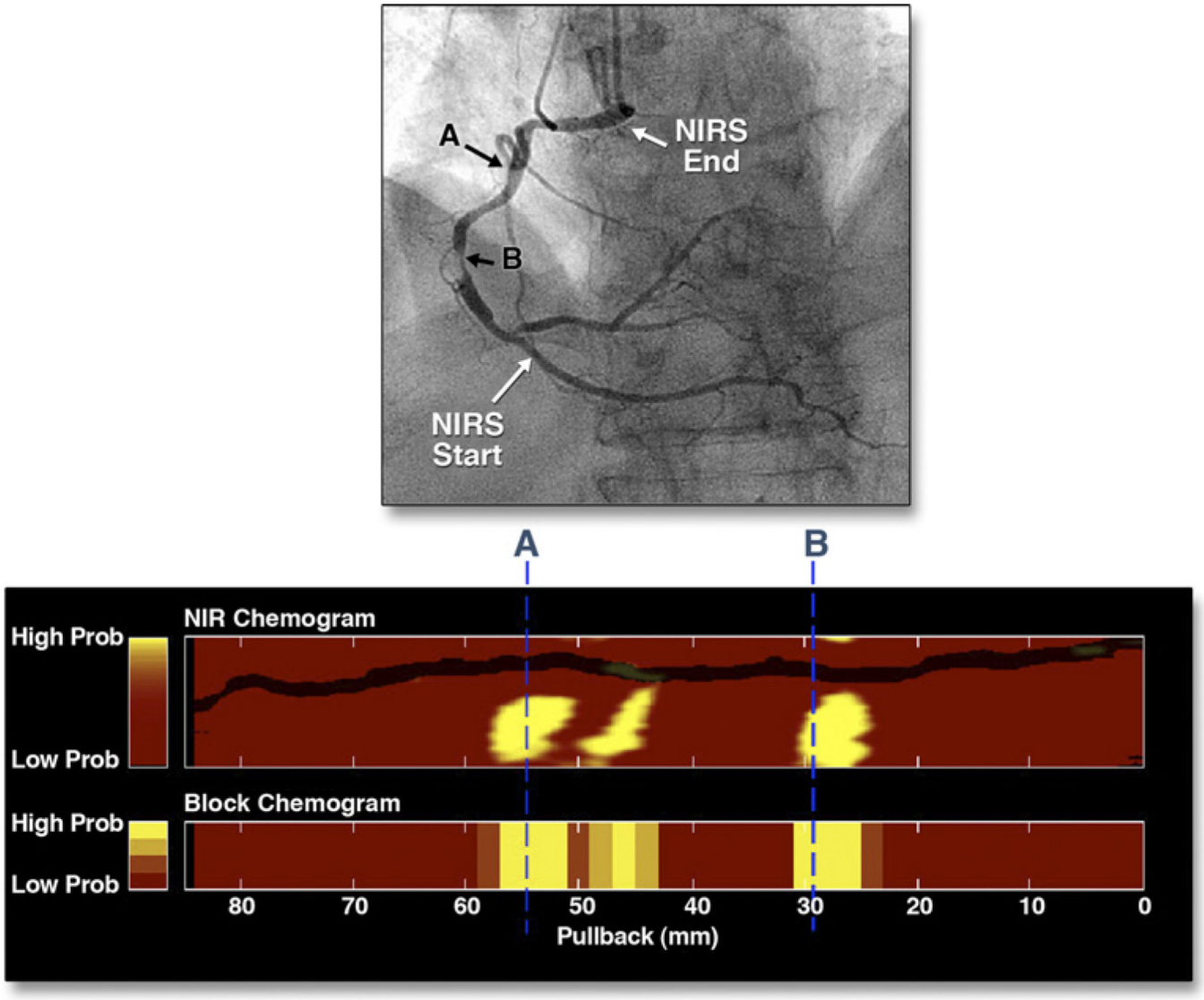

Figure 5. NIRS Scan of a and Corresponding Coronary Angiogram

(Top) Cineangiographic frame of the right coronary artery of a 68-year-old man with unstable angina. There is a severe, irregular culprit stenosis in the mid-portion of the artery. **(Bottom)** Corresponding near-infrared spectroscopy (NIRS) chemogram reveals a prominent lipid core plaque (LCP) signal between 25 and 31 mm that colocalizes with the culprit stenosis. There are 2 more proximal LCP signals between 43 and 58 mm **(A)** that probably correspond to a single plaque mass in an angiographically normal segment of the vessel. The block chemogram, which provides a summary of the data, shows the strongest LCP signals between 26 to 31 mm, 45 to 47 mm, and 51 to 57 mm. Adapted, with permission, from Waxman et al. (27).

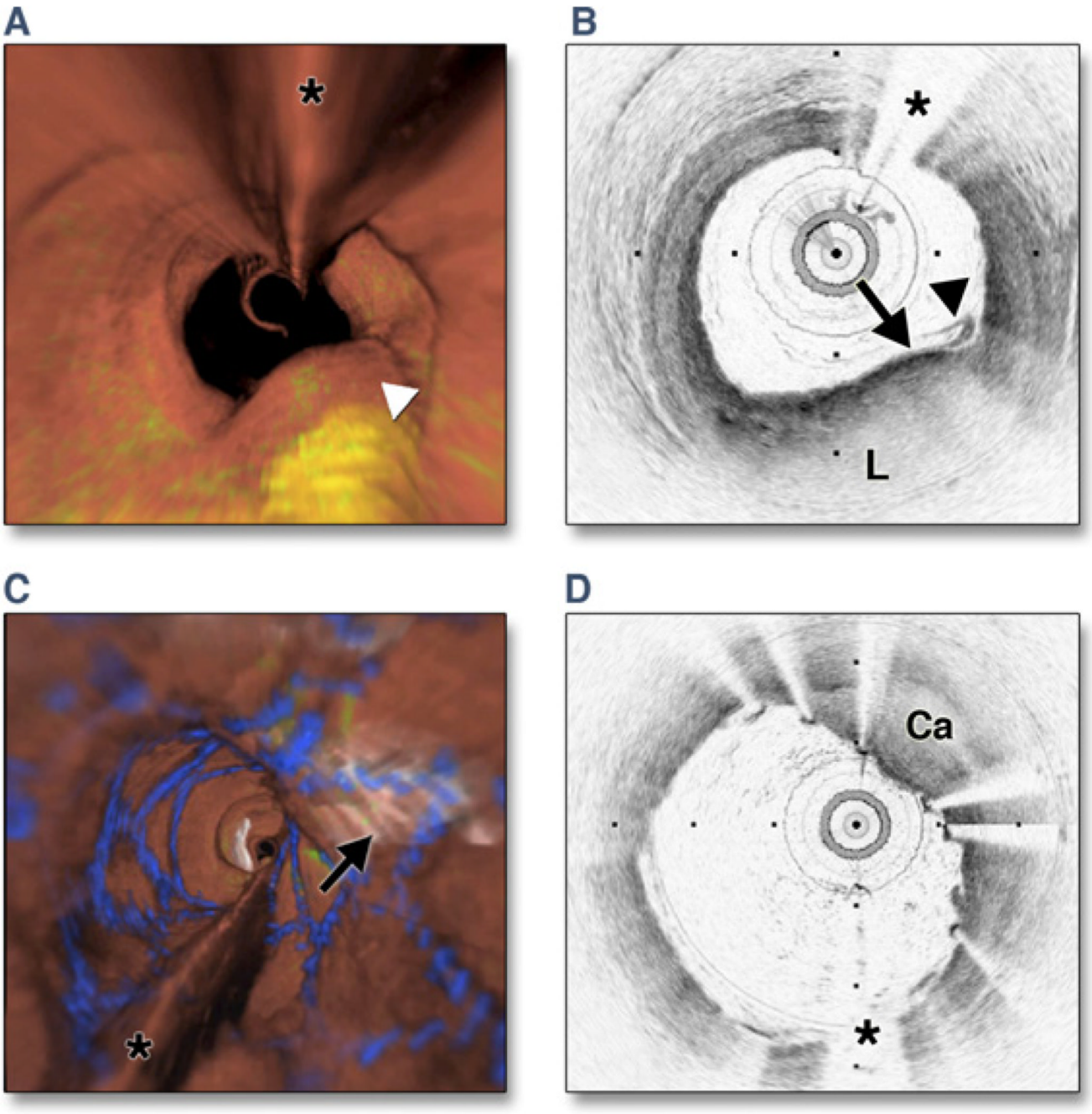

Figure 6. Optical Frequency Domain Imaging of the Left Anterior Descending Coronary Artery, Obtained In Vivo

(A) Fly-through view (proximal-distal) demonstrates a yellow, elevated lesion with scattered macrophages. **(B)** Optical frequency domain cross-sectional imaging obtained at the location of the **white arrowhead** in **(A)** shows a necrotic lipid core (L). A thin cap is present **(black arrow)** with a dense band of macrophages at the cap–lipid pool interface. A thin flap of tissue **(black arrowhead)** can be seen over the cap. Adapted, with permission, from Tearney et al. (30). **(C)** Fly-through view (proximal-distal), demonstrates a calcified lesion underneath a stent. **(D)** Optical frequency domain cross-sectional imaging obtained at the location of the **black arrow** in **(C)** shows a large calcific nodule (Ca) underneath the stent,

from 11 to 5 o'clock. **(A and C)** Artery wall in red, macrophages in green, lipid pool in yellow, stent in blue. Tick marks, 1 mm. **Asterisks** denote guidewire artifact.

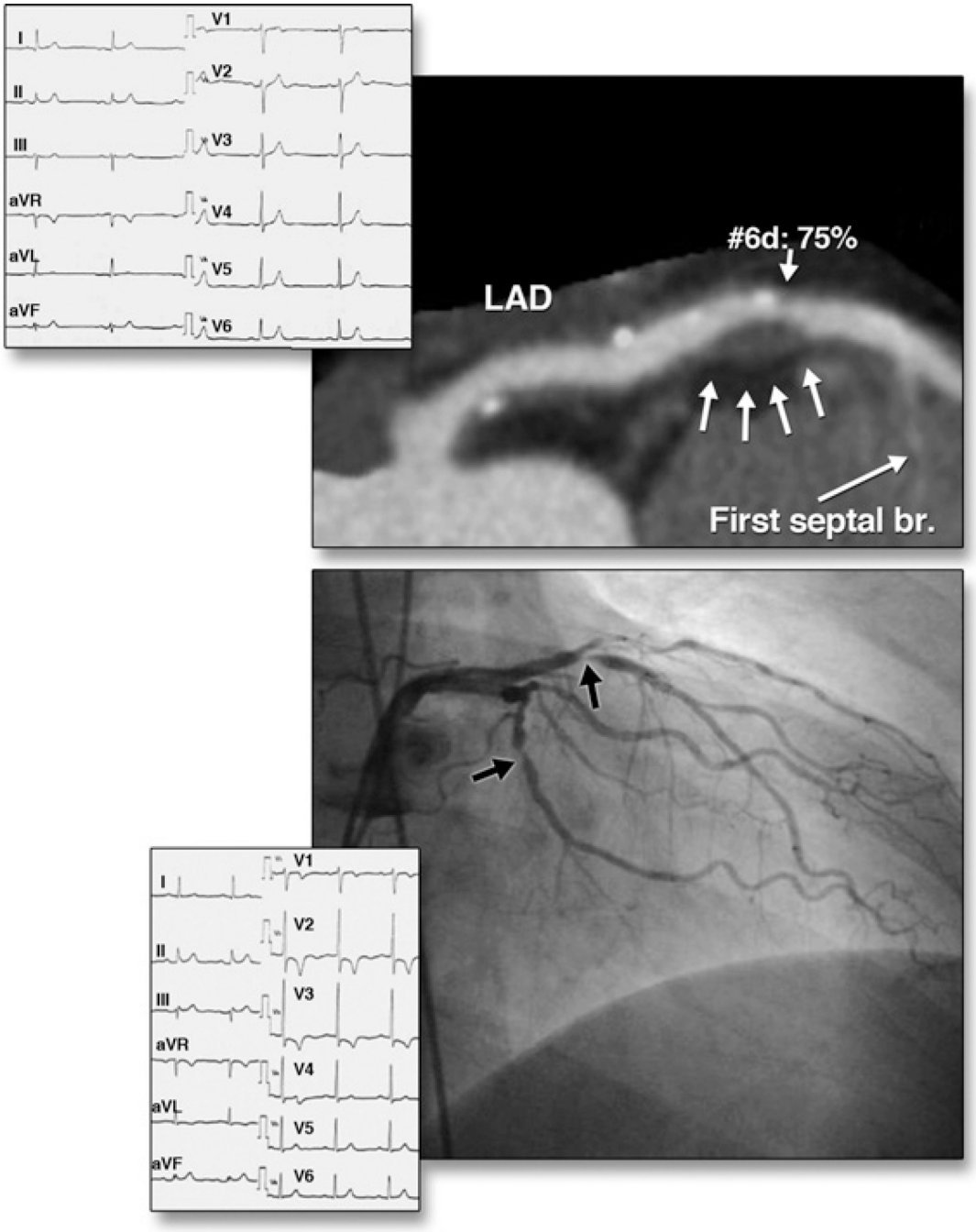

Figure 7. Morphological Characteristics on Coronary CTA of an Atherosclerotic Lesion Resulting in ACS

(Top) Curved multiplanar reformation image of the left anterior descending artery (LAD) shows positive remodeling, low-attenuation plaque, and spotty calcification at site 6 on computed tomography angiography (CTA). **(Bottom)** Acute coronary syndrome (ACS) occurred 6 months after CTA. LAD site 6 was the culprit lesion based on invasive coronary angiography. The electrocardiograms at initial presentation and during the subsequent event are shown. Reprinted, with permission, from Motoyama et al. (39).

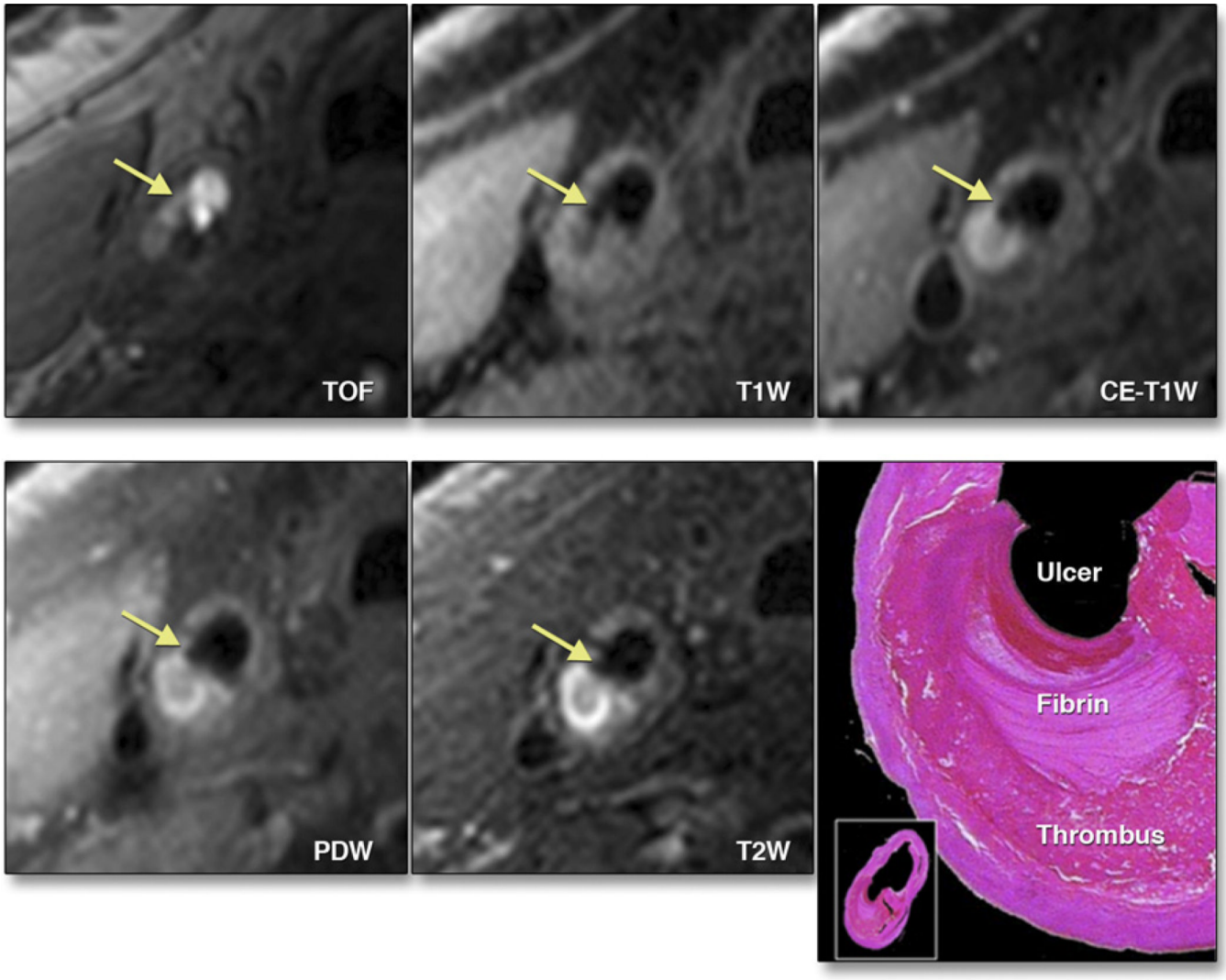

Figure 8. Morphological Characteristics of Carotid Artery Atherosclerosis Using MRI

3-T magnetic resonance imaging (MRI) of a plaque in the right common carotid artery demonstrates fibrous cap rupture with ulcer formation **(yellow arrows)**. The crescent-shaped high-signal region in the proton density-weighted (PDW), T2-weighted (T2W), and contrast-enhanced T1-weighted (CE-T1W) images correspond to a region of thrombus formation, shown on the matched histology section (hematoxylin and eosin stain). TOF = time of flight. Adapted, with permission, from Chu B, Ferguson MS, Underhill H, et al. Detection of carotid atherosclerotic plaque ulceration, calcification, and thrombosis by multicontrast weighted magnetic resonance imaging. Circulation 2005;112:e3– 4.

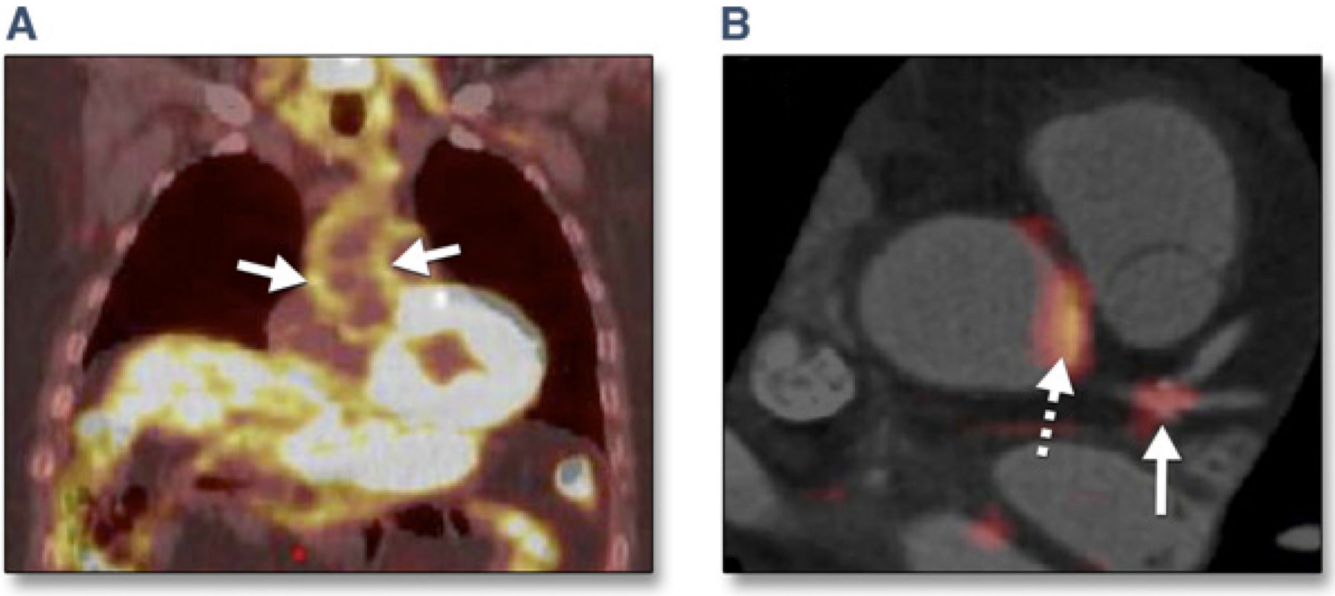

Figure 9. Imaging Arterial Inflammation Using FDG-PET

(A) Patient demonstrating enhanced aortic uptake of fluorodeoxyglucose (FDG) on positron emission tomography (PET) scan, indicating inflammation in the arterial wall due to atherosclerosis. **(B)** Co-registered FDG-PET/computed tomography images showing FDG uptake at the left main coronary artery trifurcation **(solid arrow)** in a patient with acute coronary syndrome. Aortic FDG uptake is indicated by the **dashed arrow**. In such patients, both aortic and coronary artery FDG uptake was increased compared with patients with stable coronary artery disease. Image courtesy of Dr. Zahi A. Fayad.

Table 1

Comparison of Noninvasive Assessment of Atherosclerotic Plaques in Humans

	MRI and Multicontrast MR	DCE (Gd)-MRI	USPIO MRI	FDG-PET With or Without CT	SPECT	MDCT
Vascular bed	Carotid, aorta, peripheral	Carotid, aorta, peripheral	Carotid, aorta, peripheral	Carotid, aorta, peripheral, coronary	Carotid, peripheral	Carotid, aorta, peripheral, coronary
Plaque characterization	Burden, remodeling, lipid-rich necrotic core	Inflammation, neovascularization	Inflammation	Inflammation (^{18}F-FDG)	Inflammation (Tc-99m LDL), apoptosis (Tc-99m annexin A5)	Burden, remodeling, lipid-rich necrotic core
Variability (interstudy)	5%–10%	15%	N/A	5%–7%	N/A	>20%
Statin intervention, months	3, 6, 12, 18	N/A	3	3	N/A	12
In-plane spatial resolution both directions, mm	0.5	0.5	0.5	4.5	10	0.4

[*] Statin + niacin at this time point.

CT = computed tomography; DCE (Gd) = dynamic contrast-enhanced gadolinium; FDG = fluorodeoxyglucose; LDL = ; MDCT = multidetector computed tomography; MRI = magnetic resonance imaging; PET = positron emission tomography; SPECT = single-photon emission computed tomography; Tc-99m = technetium-99m; USPIO = ultrasmall superparamagnetic iron oxide.

Table 2

Features of Different Animal Models of Atherosclerosis and Their Utility in the Validation of Emergent Imaging and Therapeutic Technologies

	Mice (60 Weeks)	Rabbit (8 Months)	Swine (~ 12 Months)
Pathology of atherosclerosis similar to humans	+	++	+++
Prominent necrotic core	++	+	+++
Positive vascular remodeling	+++	++	+++
Thinned fibrous cap	+++	++	++
Evidence of plaque rupture	+++	+	++*
Known genetic background	+++	++†	++†
Simple development method	++	++	++
Metabolic profile similar to humans	+	+	+++‡
Short development time (<6 months)	++	+++	++§
Ability to perform noninvasive imaging	++	++	++
Ability to perform invasive imaging	—	++	+++
Ability to perform systemic therapeutic interventions	++	++	++
Ability to perform invasive therapeutic procedures	—	++	+++
Development cost	+	++	+++

*Usually evident as intraplaque hemorrhage.

†The Watanabe rabbit and the FH swine have well-characterized genetic backgrounds.

‡Except for persistently low triglyceride levels.

§Lesions develop in the diabetic swine between 5 and 9 months.